International Journal of Fatigue 140 (2020) 105820

Contents lists available at ScienceDirect

International Journal of Fatigue

journal homepage: www.elsevier.com/locate/ijfatigue

Unfolding the early fatigue damage process for CFRP cross-ply laminates

Xi Li, Julian Kupski, Sofia Teixeira De Freitas, Rinze Benedictus, Dimitrios Zarouchas*

Structural Integrity & Composites Group, Faculty of Aerospace Engineering, Delft University of Technology, Kluyverweg 1, 2629HS, Netherlands

ARTICLE INFO

Keywords:
Early fatigue damage process
Damage interaction
In-situ monitoring
Digital Image Correlation

ABSTRACT

This study investigates the early fatigue damage of cross-ply carbon/epoxy laminates. The aim is to unfold the damage accumulation process, understand the interaction between different damage mechanisms, and quantify their contribution to stiffness degradation. Tension-tension fatigue tests were performed, while edge observation and DIC technique monitored the damage evolution. It was found that different accumulation process and interactive levels between transverse matrix cracks and delamination exist for specimens with similar stiffness degradation. A linear increase of stiffness degradation was observed with the increase of matrix crack density, while the growing trend of stiffness degradation converged with the increase of delamination.

1. Introduction

During in-service life, composite laminates are subjected to a variety of loads over time that induce fatigue damage and as a consequence degrade the mechanical properties of the structure. The fatigue damage levels and corresponding loading capacities are generally represented by degradation of stiffness [1–3] and variation of self-generated temperature [4–6] from the macroscopic perspective. In view that stacking sequences and material properties of laminates determine if thermo-mechanical effects are detectable, measuring of temperature variation is less universal than that of stiffness variation. A three-stage process in a rapid-slow-rapid manner has been reported as the representative stiffness degradation for laminates under fatigue loading, as illustrated in Fig. 1 [1–3]. Considering that the stiffness degrades significantly in early fatigue life, it would be of great interest to firstly put emphasis on early fatigue damage, uncovering which damage mechanisms accumulate, how they interact and affect the stiffness degradation. This may also help gain a better insight of the significant scatter phenomenon about failure life for composites and further pave the way to probabilistic predictions of fatigue life with physics of damage involved.

Early fatigue damage usually refers to damage within the first 10% of the fatigue life that distributes throughout the entire laminate leading to stiffness degradation and specimen heating [7,8]. As is matrix-dominant, it contains two kinds of mechanisms: off-axis matrix cracks and delamination.

For coupon-level laminates, off-axis matrix cracks usually generate from free edges due to stress concentration which then propagate through the fibre direction [9,10]. Their initiation, driven by local maximum principal stress and local hydrostatic stress in the matrix [11], appears at the first few cycles when the maximum stress under fatigue loading is higher than the threshold stress to induce off-axis matrix cracks under quasi-static loading, otherwise the initiation delays [9]. Considering randomly-distributed micro-defects, such as voids, inclusion of foreign particles and local fibre–matrix debonding, which usually occurs during the manufacturing process [12], the resistance to off-axis matrix cracks under fatigue loading varies among local regions of a laminate [13]. As a result, the fatigue life, when the first off-axis matrix crack occurs, usually presents a significant scatter band, especially for low stress levels [10,11,14,15]. During the subsequent fatigue cycles, the number of off-axis matrix cracks gradually increases up to a saturation state, which is also termed as Characteristic Damage State (CDS) [1,2,16]. It has been proposed that the CDS is independent to loading conditions and only depends on laminate layups, geometries and material properties [1,2], while experimental evidences [16–18] showed that both fatigue life and matrix crack density at CDS depend on stress levels and loading control modes, and they can be even different among specimens under the same loading condition [15].

Delamination is another damage mechanism that appears at the early fatigue life of a laminate and it usually originates from the tips of off-axis matrix cracks or free edges due to the high inter-laminar stress concentrations [1,5]. Initially, it was hypothesized that, delamination initiate after CDS [1], however, experimental observations [2] showed that before reaching CDS, delamination may appear specifically at regions with high density of off-axis matrix cracks. Furthermore, Hosoi et al. [19] reported that edge delamination initiates and propagates before or simultaneously with the initiation of off-axis matrix crack under low stress level. Xu et al. [20] proposed that the constraining effect of uncracked plies and material properties of cracked plies

* Corresponding author.
E-mail address: D.Zarouchas@tudelft.nl (D. Zarouchas).

https://doi.org/10.1016/j.ijfatigue.2020.105820
Received 20 April 2020; Received in revised form 3 July 2020; Accepted 4 July 2020
Available online 10 July 2020

Nomenclature

Symbols	Descriptions [Units]
A_C	normalized area of DIC-based transverse strain concentration [–]
A_{loss}	loss of amplitude [dB]
a	a fitted parameter in the expression of ρ(N), also termed as crack growth factor [mm^{-1}]
b	a constant in the expression of ρ(N) which is 7 × 10^{-5} and 5.46 × 10^{-5} for specimens of Group 1 and Group 2 respectively [–]
D	stiffness degradation [–]
D_{TC}	decoupled stiffness degradation contributed by transverse matrix cracks [–]
D_{del}	decoupled stiffness degradation contributed by delamination [–]
d_r, d_{rs}	delamination ratio, delamination ratio at CDS [–]
$\Delta d_r/\Delta N$	growth rate of delamination ratio in terms of fatigue life [cycle^{-1}]
E_0	longitudinal stiffness obtained from the first tensile loading ramp [GPa]
E_I	longitudinal stiffness at the end of Stage I [GPa]
E_N	longitudinal stiffness at the N^{th} cycle [GPa]
E_N/E_0	normalized longitudinal stiffness at the N^{th} cycle [–]
I_r	inter-laminar crack ratio [–]
L_{l1}, L_{l2}	total length of inter-laminar cracks located at each interface of the left edge [mm]
L_{r1}, L_{r2}	total length of inter-laminar cracks located at each interface of the right edge [mm]
N	number of cycles [cycle]
N_{c1}, N_{c2}, N_{c3}	Fatigue life consumed by the slow generation of transverse matrix cracks at the beginning of tests for specimen #2–1, #2–2 and #2–3 respectively [cycle]
N_c	minimum value among N_{c1}, N_{c2} and N_{c3} [cycle]
N_s	fatigue life at CDS [cycle]
$\bar{\varepsilon}_{xx}$	average axial strain [–]
ε_{yy}, $\bar{\varepsilon}_{yy}$	transverse strain, average transverse strain [–]
ν	in-situ Poisson's ratio [–]
ρ, ρ(N)	matrix crack density, matrix crack density as a function of N [mm^{-1}]
ρ_s	saturated matrix crack density [mm^{-1}]
$\Delta\rho/\Delta N$	growth rate of matrix crack density in terms of fatigue life [(cycle × mm)$^{-1}$]
σ_{xx}	axial stress [MPa]

Abbreviations

CDS	characteristic damage state
CFRP	carbon fibre reinforced polymer
DIC	digital image correlation
IS	interactive scheme
NIS	non-interactive scheme
UD	unidirectional
UTS	ultimate tensile strength

determine whether off-axis matrix cracks would initiate before or after the onset of delamination. Pakdel and Mohammadi [2] and Shen et al. [17] concluded that delamination could postpone or prevent further generation of off-axis matrix cracks at neighbouring regions. Further, based on the stress state analysis of co-existing off-axis cracks and delamination, Talreja [21] found that the maximum axial stress in the middle of adjacent cracks at the off-axis plies decreases with the increase of delamination length, causing the reduction of driving force for producing new off-axis matrix cracks. These different occurring sequences of the off-axis matrix crack initiation, saturation and delamination initiation reflect multiple levels of interaction behaviours

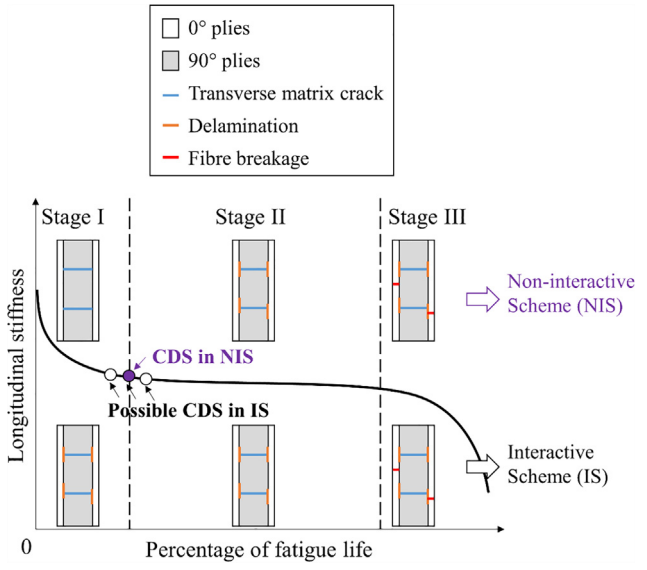

Fig. 1. Three-stage stiffness degradation process for cross-ply laminates under tensile-tensile fatigue loading and corresponding damage accumulation process with and without the interactions between transverse matrix cracks and delamination.

Table 1
Material properties of the UD lamina manufactured by Hexply® F6376C-HTS (12 K)-5-35% Prepreg [38].

Longitudinal modulus	E_{11T} = 142 GPa
Transverse modulus	E_{22T} = E_{33T} = 9.1 GPa
In-plane shear modulus	G_{12} = G_{13} = 5.2 GPa
Transverse shear modulus	G_{23} = 3.5 GPa
Longitudinal strength	X_T = 2274 MPa, X_C = 1849 MPa
Transvers strength	Y_T = 102 MPa, Y_C = 255 MPa
In-plane shear strength	S_{12} = S_{13} = 63 MPa
Transverse shear strength	S_{23} = 35 MPa
In-plane Poisson ratio	ν_{12} = ν_{13} = 0.27
Transverse Poisson ratio	ν_{23} = 0.30

Note: $_T$ - tensile; $_C$ - compression.

between both damage mechanisms.

The accumulation and interaction of fatigue damage produce cyclic-dependent deformation, accompanied with time-dependent deformation (*i.e.* creep) induced by the viscoelasticity of matrix [22]. Both types of deformation contributes to significant stiffness degradation and it appears within a short duration of fatigue life at Stage I, followed by Stage II that occupies most of the fatigue life where the stiffness almost remains constant and Stage III with sudden drop of stiffness, as presented in Fig. 1. Different phenomenological models have been established to describe the degradation process [23], and they were also implemented afterwards into fatigue progressive damage frameworks for fatigue life prediction [24,25]. In some prior studies [1,5], off-axis matrix cracks were founded to be the only damage mechanism at Stage I, after which delamination occur at Stage II followed by fibre breakage at Stage III. As the non-interactive scheme about fatigue damage accumulation, the transition point of stiffness degradation from Stage I to Stage II is ideally at CDS (see Fig. 1). For this case, off-axis matrix cracks are the only contributor to stiffness degradation within Stage I [16,17,26]. Accordingly, in the progressive fatigue damage model proposed by Shokrieh *et al.*, a gradual stiffness degradation of 90 plies is performed to reflect the transverse matrix crack evolution of cross-ply

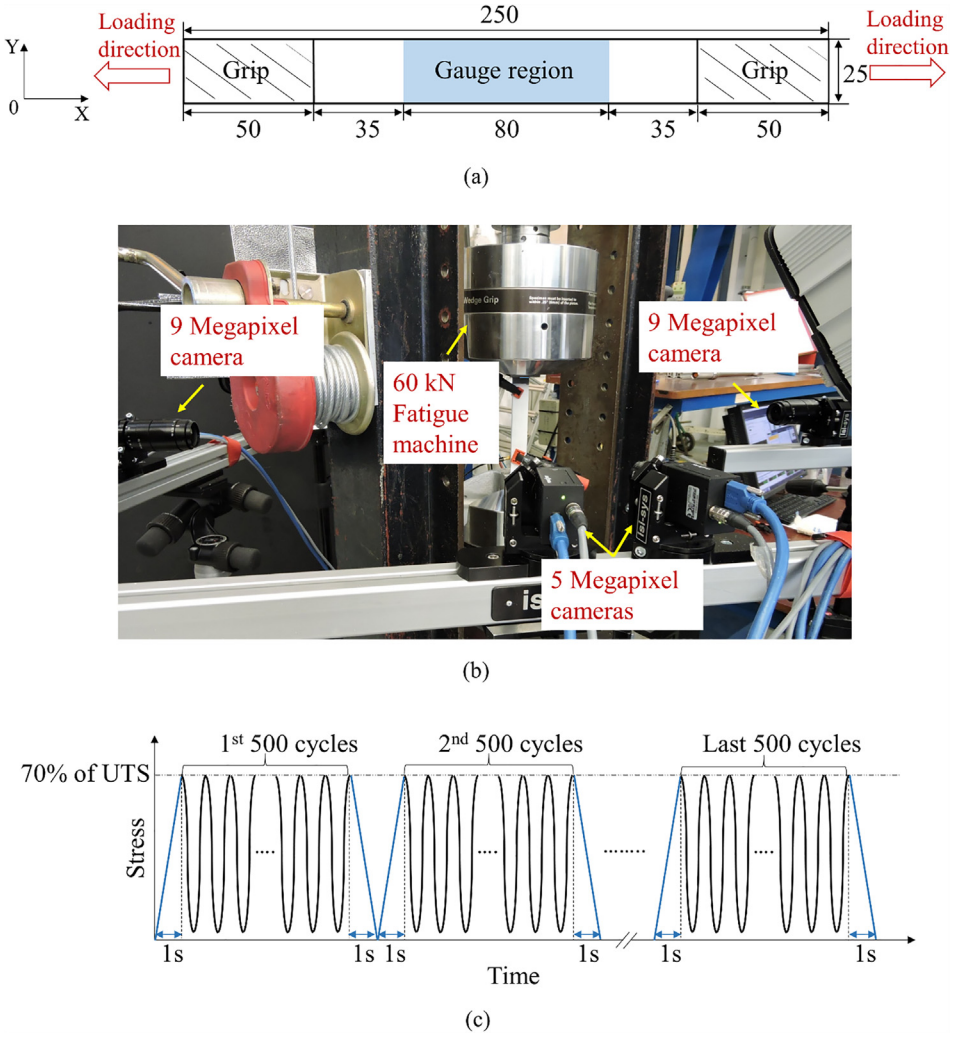

Fig. 2. The schematic diagram of specimen dimensions, gauge region and clamping area (in [mm]), and loading direction (a); Test set-ups (b); Loading pattern of fatigue test (c).

laminates within Stage I, which is then terminated by a sudden 90-ply discount when reaching CDS [27,28]. Wharmby *et al.* observed a linear relationship between the normalized stiffness and matrix crack density [29]. However, in case that both damage mechanisms interact within Stage I, at which moment CDS occurs: within Stage I, at the transition point of the first two stages or within the Stage II, as marked in Fig. 1, and how off-axis matrix cracks and delamination contribute to stiffness degradation individually have not been studied yet. A fundamental understanding towards this direction could be achieved by performing experimental campaigns aiming to isolate each damage mechanism and identify the moments of interaction.

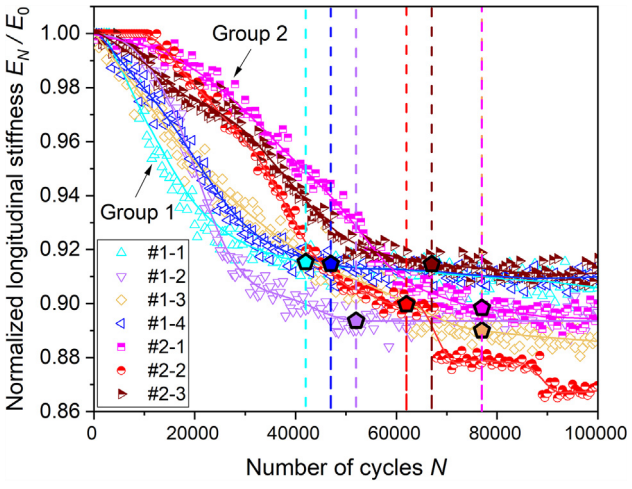

Fig. 3. Normalized longitudinal stiffness versus number of cycles for cross-ply laminates within 10^5 cycles.

So far, different damage monitoring techniques have been involved to investigate the progressive damage behaviour of composites under fatigue loading. For Glass Fibre Reinforced Polymer, due to their high transparency, in-situ monitoring of matrix crack density and delamination area has been successfully achieved by transmitted light photography combining with post image processing [17,26,29–31]. However, this technique is not applicable for non-transparent composites like Carbon Fibre Reinforced Polymer (CFRP), and a challenge still remains for the detection of delamination. A common practice is to perform multiple interruptions of the fatigue testing for in-situ/ex-situ crack replica or microscopy inspections on edges [2,3,32,33], and ex-situ examination of internal damage (*i.e.* off-axis matrix cracks towards the width direction and delamination) using X-radiography [18,19,33,34], which actually affects both fatigue life and damage accumulation process of composites [35,36]. Therefore, experimental improvements towards in-situ damage monitoring, especially for delamination, are needed for CFRP composites.

In the present study, edge observation and Digital Image Correlation

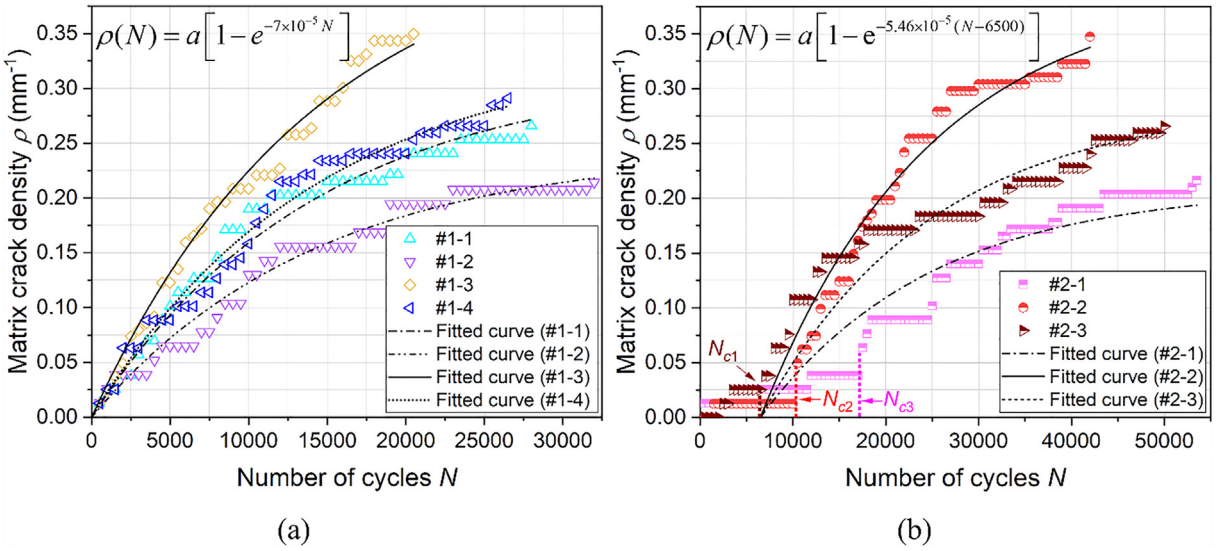

Fig. 4. Evolution of matrix crack density with fatigue life until the saturation of transverse matrix cracks for specimens of Group 1 (a) and Group 2 (b).

(DIC) techniques were used under tensile-tensile fatigue loading to achieve in-situ damage monitoring of cross-ply CFPR laminates. Stiffness degradation and accumulation of both damage mechanisms (*i.e.* transverse matrix cracks and delamination) were characterized and quantified in the early fatigue life. The objectives are to explore the accumulation and interaction of early fatigue damage occurred at Stage I, and to further understand the contribution of each damage mechanism to stiffness degradation.

2. Experimental methods

2.1. Material and specimens

The specimens used in the present work were fabricated using unidirectional (UD) Prepreg named Hexply® F6376C-HTS(12 K)-5-35% with high tenacity carbon fibres (Tenax®-E-HTS45) and a tough epoxy matrix (Hexply® 6376) involved. This UD Prepreg system has a nominal ply thickness of 0.125 mm and a nominal fibre volume content of 58%. The laminated panels of 300 mm × 300 mm size and stacking sequence of $[0_2/90_4]_S$ were cured inside an autoclave according to recommendation from Hexcel [37], and the material properties of UD lamina in cured condition is listed in Table 1 [38]. Based on ASTM D3479/D3479M-19 standard [39], the cured panels were cut into rectangular shape with 250 mm × 25 mm size using a water-cooled diamond saw and both ends of specimens with 50 mm length were glued with thick paper tabs using cyanoacrylate adhesive to increase clamping grip (see Fig. 2(a)).

2.2. Test set-up

Seven specimens were tested under tension–tension fatigue loading on a 60 kN hydraulic fatigue machine at room temperature. The test set-up and a schematic representation of applied loading profile, containing the repetitive cyclic loading blocks and the tensile loading–unloading ramps, are shown in Fig. 2(b) and (c), respectively. Constant amplitude of sinusoidal waves, with maximum stress of 507 MPa (70% of UTS), stress ratio 0.1 and frequency 5 Hz were applied, while the tensile loading and unloading ramps were applied before and after every 500 cycles with the rate of 19 kN/s. The maximum stress was determined based on the results of static tensile and preliminary fatigue tests. During tests, two 9 Megapixel cameras with 50 mm-focal-length lens were placed at left and right sides of the clamped specimens to monitor the damage on both edges. The edge surfaces of each specimen were covered with thin white paint in order to enhance the white-black contrast of cracked and uncracked regions. Furthermore, the exterior 0-ply was painted with a white base coat and printed with black dots using a speckle roller with the dot size of 0.18 mm. A second pair of 5 Megapixel cameras with 23 mm-focal-length lens was placed in the front of specimens to measure the in-plane strain field. All cameras were triggered simultaneously during the tensile loading–unloading ramps to capture images every 50 ms. Tests stopped when reaching 10^5 cycles, which guarantees that the stiffness degradation develops through the Stage I and approaches to the stable phase of Stage II. Two specimens were scanned by an ultrasonic C scanner to detect the delamination area after test.

A user-defined MATLAB image-analysis code was developed to count the number of transverse cracks at 90 plies and measure the length of inter-laminar cracks at 0/90 interface. As for the DIC

Table 2
The value of crack growth factor a and related R-square.

Specimen	Group 1				Group 2		
	#1–1	#1–2	#1–3	#1–4	#2–1	#2–2	#2–3
a	0.316	0.244	0.447	0.336	0.210	0.394	0.287
R-Square	0.970	0.976	0.985	0.978	0.904	0.968	0.827

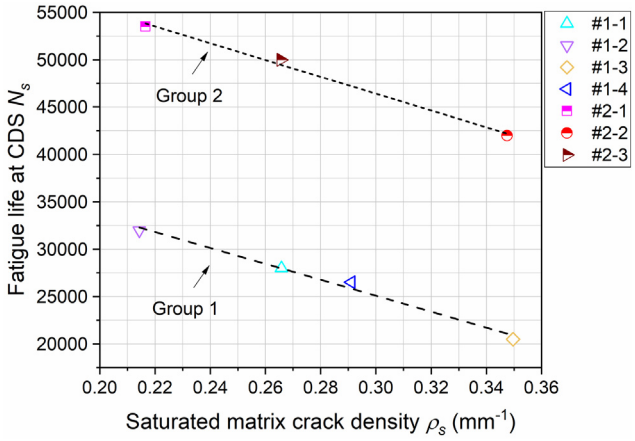

Fig. 5. The relationship between saturated matrix crack density and fatigue life at CDS for two groups of specimens.

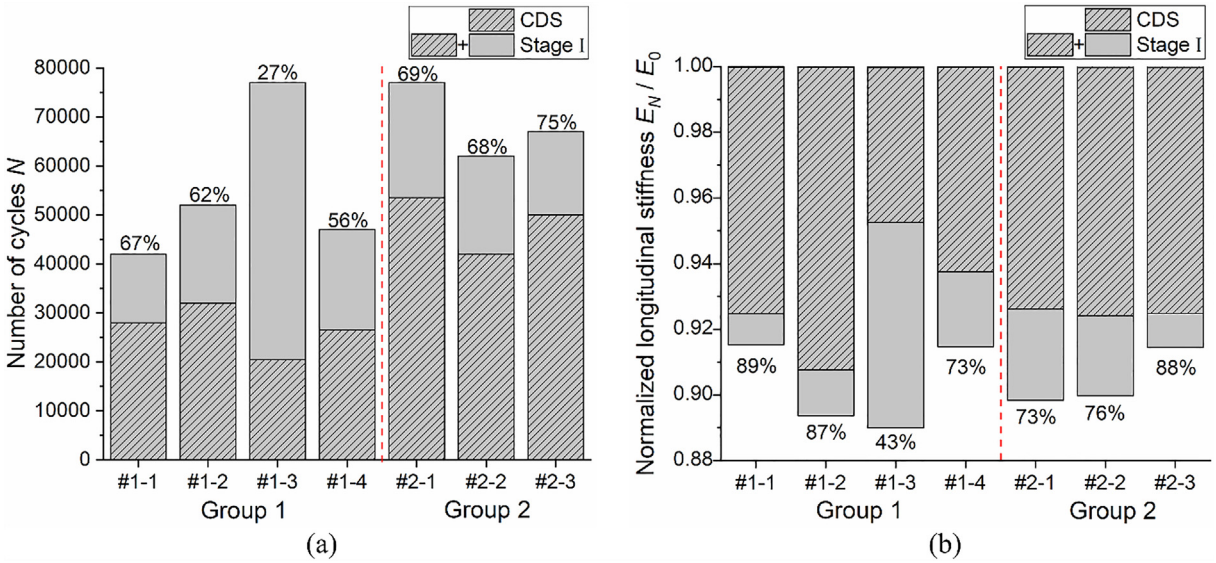

Fig. 6. Fatigue life (a) and stiffness degradation (b) consumed at CDS and the end of Stage I, as well as the percentages occupied at CDS in comparison with the end of Stage I.

calculations, a subset size of 29 pixels and step size of 7 pixels were fixed for all specimens. The interest area was fixed at gauge region with ~ 80 mm length for both edge damage and DIC (see Fig. 2(a)).

3. Results and discussions

3.1. Longitudinal stiffness

Stress/strain hysteresis loops are usually used to obtain secant stiffness and dynamic stiffness (also termed as fatigue stiffness [40]) with and without considering the creep effect respectively [41]. In the present study, dynamic stiffness along the axial direction was calculated every 500 cycles, based on the slope of σ_{xx} and $\bar{\varepsilon}_{xx}$ for each tensile loading ramp (see Fig. 2(c)), where σ_{xx} is the axial stress and $\bar{\varepsilon}_{xx}$ is the average axial strain as calculated by the DIC. Fig. 3 plots normalized longitudinal stiffness E_N/E_0 in function of number of cycles N. E_0 is the initial axial stiffness obtained from the first tensile loading ramp (see Fig. 2(c)) and E_N is the degraded axial stiffness at cycle N. Furthermore, the transition points from Stage I to Stage II, quantified as the moment when E_N/E_0 decreases less than 0.001 every 5 data points, are also marked in the pentagon shape (see Fig. 3)

Until the end of Stage I, stiffness degraded about 8% to 11% and a slower decreasing rate was shown for specimens of Group 2 than that of Group 1 (see Fig. 3). In a linear-elastic material system, energy dissipation can be derived from stiffness degradation under constant load or displacement [42]. Based on this, a slower increasing rate of dissipated energy can be inferred for specimens of Group 2 than Group1. The reason for different rates of stiffness degradation and dissipated energy between both groups is the damage accumulation process which should be further explored.

3.2. Accumulation process of early fatigue damage

In the present study, early fatigue damage is focused at Stage I, which contains off-axis matrix cracks, also named as transverse matrix cracks for cross-ply laminates, and delamination.

3.2.1. Transverse matrix cracks

Transverse matrix cracks initiated within the first 500 cycles for most of specimens, except specimen #2–2 and #2–3 which delayed to the third and fifth 500 cycles respectively. During the tests, most of transverse matrix cracks were extended throughout the entire width immediately due to the thick 90-ply block in the middle of laminates. To further quantify the accumulation process, matrix crack density ρ was introduced, which was calculated by the average number of transverse matrix cracks at both edges divided by the gauge length (~80 mm). Fig. 4 presents the matrix crack density ρ as a function of number of cycles N until CDS for two groups of specimens. Compared with Group 1, ρ at Group 2 started with a particularly slow increase up to certain cycles (*i.e.* N_{c1}, N_{c2} and N_{c3} for specimen #2-1, #2-2 and #2-3 respectively, as marked in Fig. 4(b)), after which the growing trends were suddenly accelerated and then the similar increasing trends as Group 1 was observed. This difference is caused by the generally higher fatigue resistance of specimens in Group 2 than that in Group 1. To establish a phenomenological relation between ρ and N, one fitting function was selected as follows:

$$\rho(N) = a[1 - e^{-b(N-N_c)}]$$

where a, b and N_c are model parameters. Here, N_c is used to eliminate the initial section where slow crack generation appeared at the beginning of tests and b is regarded as constant among specimens of each group. For Group 1, $N_c = 0$ and $b = 7 \times 10^{-5}$; for Group 2, $N_c = \min\{N_{c1}, N_{c2}, N_{c3}\} = 6500$ and $b = 5.46 \times 10^{-5}$. The final fitting functions and curves for each group are shown in Fig. 4. Obviously, only a determines the growing trend of ρ(N) and is defined as a crack growth factor in the present study. Table 2 listed the value of a and related R-square.

Despite similar stiffness degradation within each group, the accumulation process of transverse matrix cracks is different (see Fig. 4), further resulting in the scatter of saturated matrix crack density ρ_s and fatigue life N_s at CDS. Fig. 5 shows linear relationships between ρ_s and N_s. For both groups, the higher the ρ_s was, a smaller number of fatigue cycles were needed to reach CDS. The decreasing trends of N_s with ρ_s were similar among both groups. In addition, ρ_s ranged from around 0.21 to 0.35 mm^{-1} while the difference of N_s was about 10,000 cycles among specimens of each group.

Fig. 6 presents number of cycles N and normalized longitudinal stiffness E_N/E_0 at CDS and at the end of Stage I. For most specimens, accumulation of transverse matrix cracks consumed 56%-75% of fatigue life within Stage I, while 73–89% of stiffness degradation was occurred until CDS, except specimen #1-3 for which the accumulation of matrix crack consumed 27% and 43% of the fatigue life and stiffness up to the end of Stage I. The results indicate that a different damage mechanism, e.g. delamination, occurred within Stage I and contributed

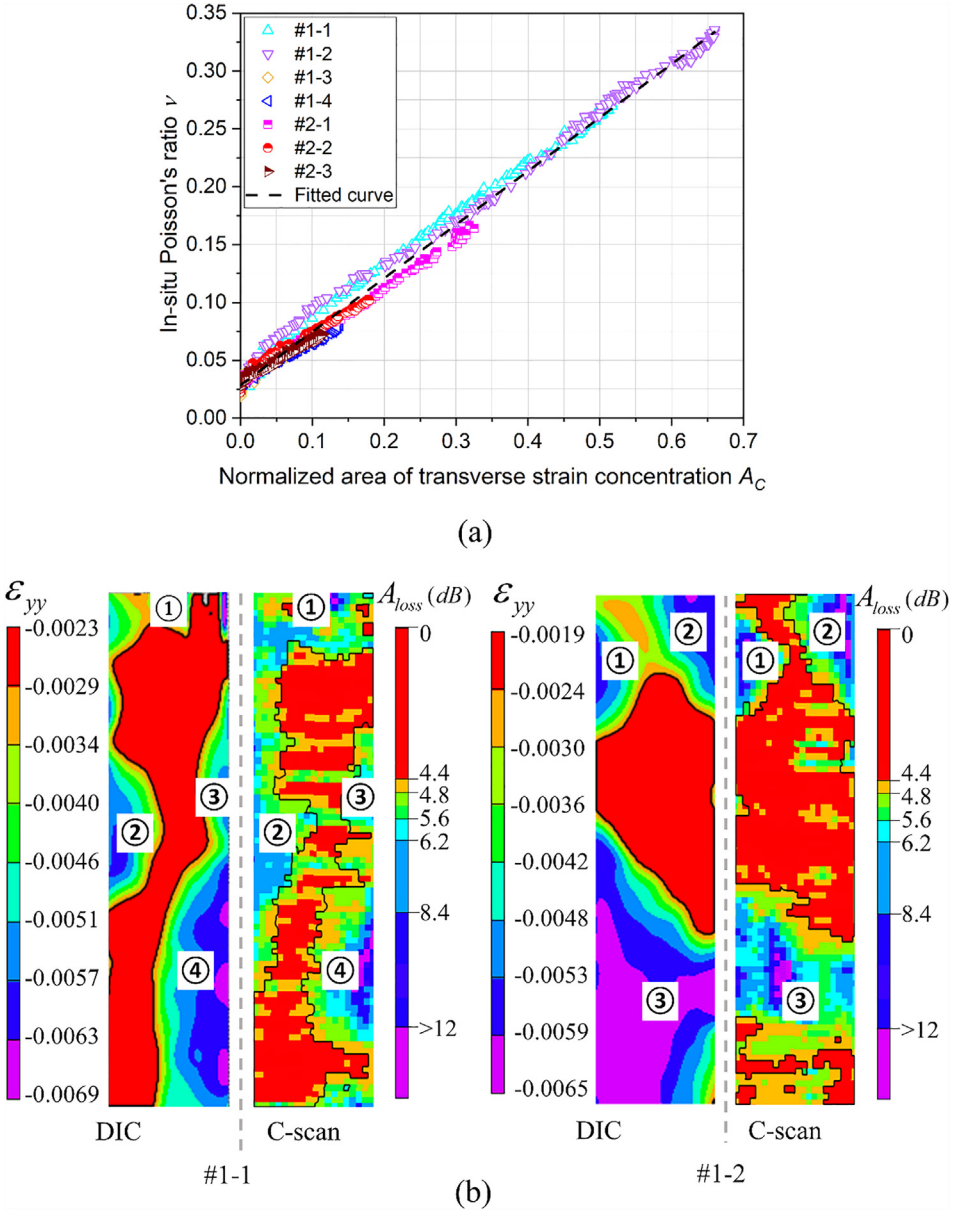

Fig. 7. In-situ Poisson's ratio versus normalized area of transverse strain concentration (a); Correlation of transverse strain concentrations and delamination at numbered local regions at 10^5 cycles (ε_{yy} – transverse strain; A_{loss} – loss of amplitude) (b).

to stiffness degradation. Therefore, it would be of great interest to investigate when delamination initiates and understand how it interacts with transverse matrix cracks and degrades stiffness.

3.2.2. Delamination

Oz *et al.* observed Poisson contraction and transverse strain concentrations through DIC at the exterior surface of quasi-isotropic CFRP laminates when delamination was generated at interfaces [43]. Following this observation and aiming at developing a DIC-based parameter to describe the delamination accumulation inside the CFRP laminates, the relations among transverse strain concentrations, Poisson contraction and delamination are further explored hereafter.

Fig. 7(a) shows a linear growth of in-situ Poisson's ratio $\nu$with the normalized area of transverse strain concentration A_C at the DIC interest area for all specimens. Here, ν is calculated by $-\frac{\bar{\varepsilon}_{yy}}{\bar{\varepsilon}_{xx}}$, where $\bar{\varepsilon}_{yy}$ and $\bar{\varepsilon}_{xx}$ are the average transverse and axial strains of the exterior 0-ply respectively. A_C is obtained by the total area of transverse strain concentration divided by the DIC measurement area. The threshold of transverse strain at the concentration region is quantified as the minimum value of transverse strain when ν starts to increase. Moreover, Fig. 7(b) correlates the delamination area from C-scanning with transverse strain concentration area from DIC at numbered local regions for specimen #1-1 and #1-2 after tests stopped at 10^5 cycles, which indicates that transverse strain concentration area can represent the delamination area. Based on all-mentioned above, in-situ Poisson's ratioν can be used to describe the accumulation process of delamination.

Inter-laminar cracks originated at tips of transverse matrix cracks, and then they propagated along 0/90 interfaces with the increase of displacement at the transverse matrix crack surfaces, which also affected the stiffness degradation process as Qi *et al.* mentioned [13]. Here, inter-laminar cracks ratio I_r, obtained by the average of max{ L_{r1}, L_{r2} } and max{ L_{l1}, L_{l2} } and divided by the gauge length (~80 mm), was used to express the accumulation of inter-laminar cracks. L_{r1}, L_{r2} are the total length of inter-laminar cracks located at each interface of the right edge and similarly L_{l1}, L_{l2} were for the left edge. Fig. 8(a)–(b) present the evolution of ν and I_r as a function of number of cycles while the

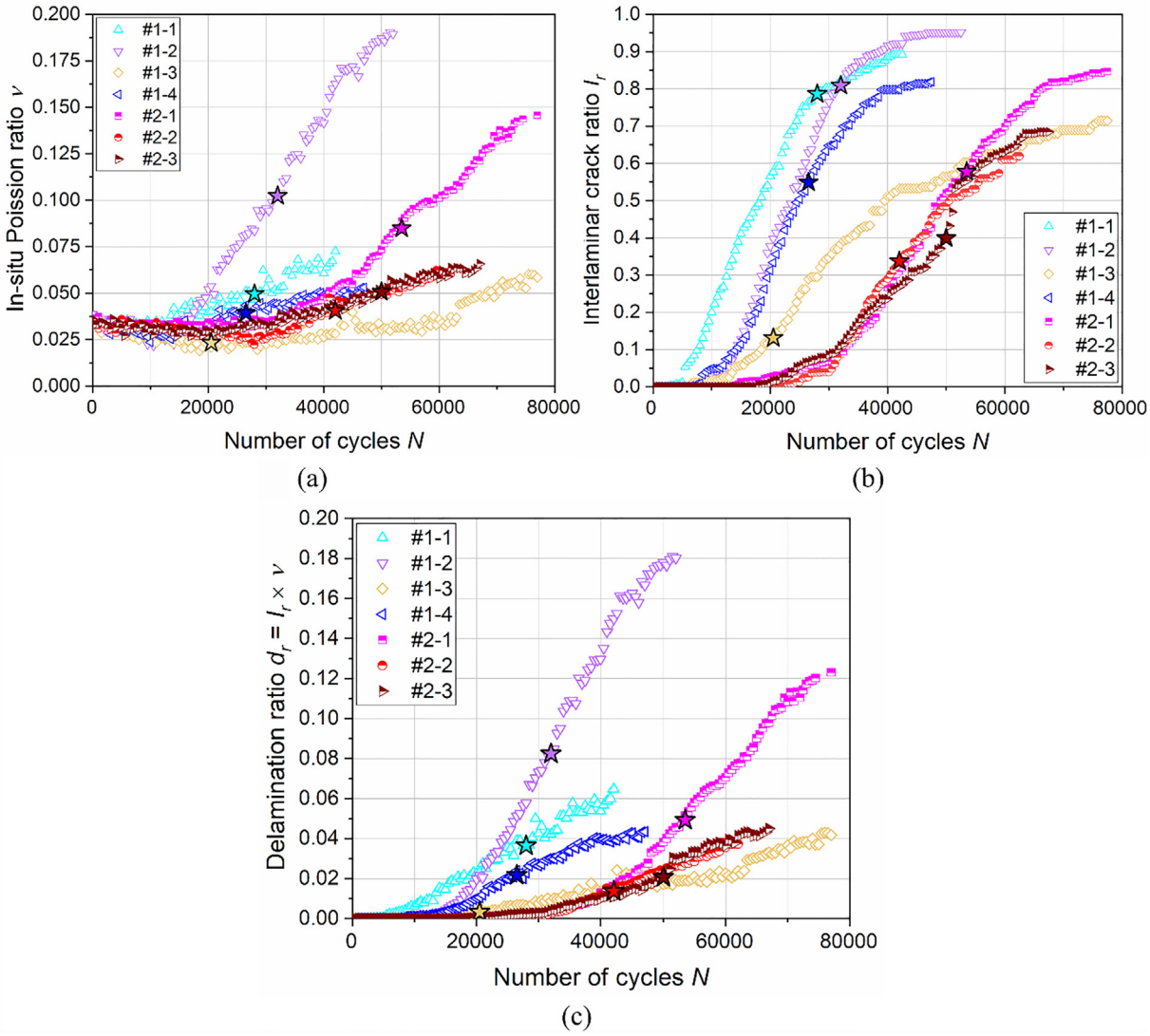

Fig. 8. The evolution of in-situ Poisson's ratio (a), inter-laminar crack ratio (b) and delamination ratio (c) with number of cycles at Stage I.

stars pinpoint the CDS. The in-situ Poisson ratio ν remained stable at the beginning and then continuously increased due to the expansion of transverse strain concentration region, while I_r experienced a slow-rapid-slow growing trend. For most of specimens, ν ranged from around 0.025 to 0.05 until the saturation of transverse matrix cracks (see Fig. 8(a)) and the corresponding maximum A_C was around 0.05 (see Fig. 7(a)) meaning that only 5% of gauge region delaminated. On the contrary, except specimen #1-3, inter-laminar cracks at edges propagated more than ~35% of gauge length until CDS (see Fig. 8(b)). These phenomena indicate that delamination propagated faster along the length than within the width of the specimens, as reported by O'Brien [44]. In view that delamination is more likely to concentrate near the edges rather than propagate inside the specimens before CDS, in-situ Poisson's ratio ν is not capable to reflect the delamination propagation during this period.

As a result, the delamination ratio d_r, calculated by $\nu \times I_r$, is proposed hereafter to represent the accumulation process of delamination along both length and width directions, as presented in Fig. 8(c). Compared with Group 2, an earlier increase of d_r was observed at Group 1, which indicates specimens with faster stiffness degradation at Stage I accompanied with earlier accumulation of delamination.

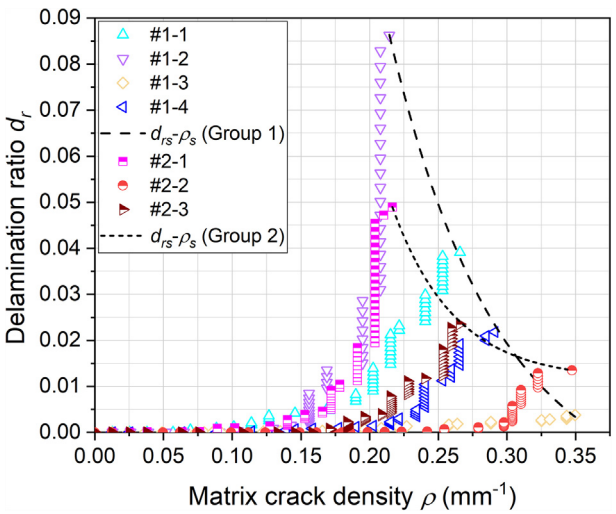

Fig. 9. The increase of matrix crack density with delamination ratio before CDS.

3.3. Interaction between transverse matrix cracks and delamination

For all specimens at CDS, the inter-laminar cracks occupied around 15%-80% of the gauge length (see Fig. 8(b)), while the delaminated

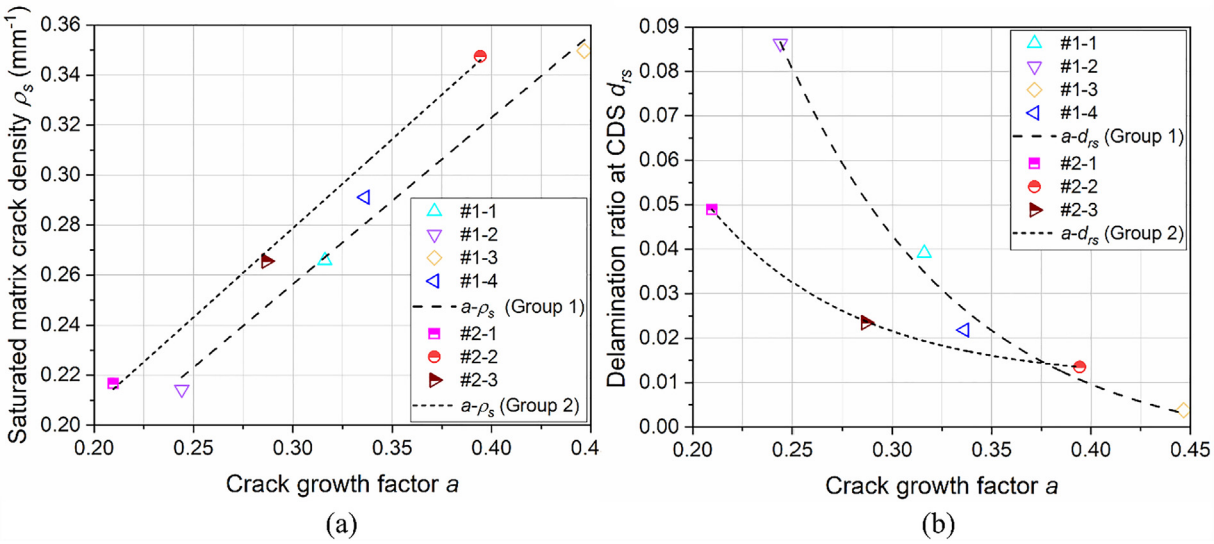

Fig. 10. The plots of proposed crack growth factor with saturated matrix crack density (a) and delamination ratio at CDS (b).

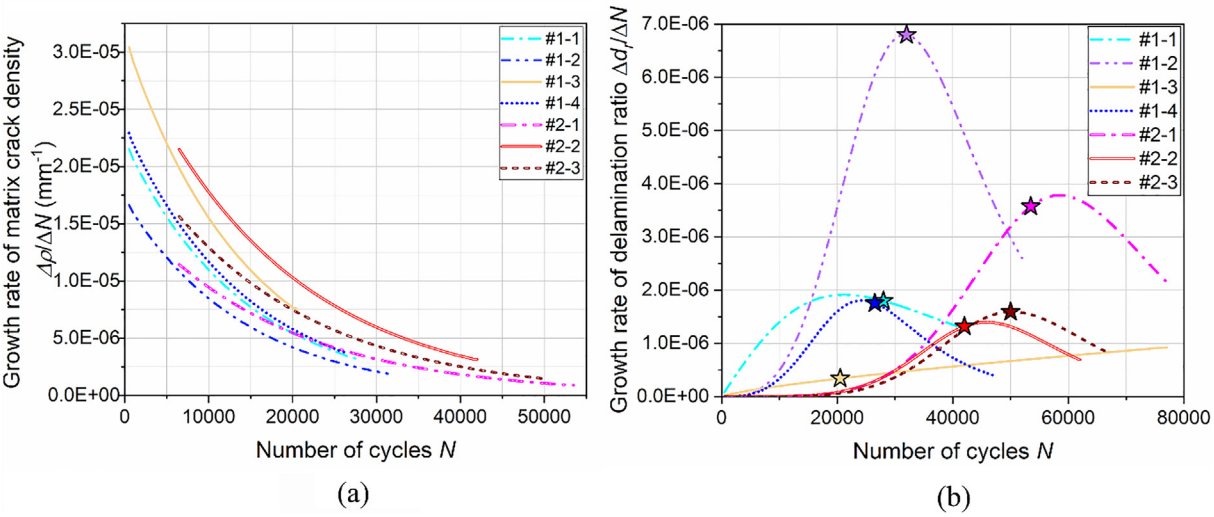

Fig. 11. The growth rate of matrix crack density (a) and delamination ratio (b) with the increase of fatigue life.

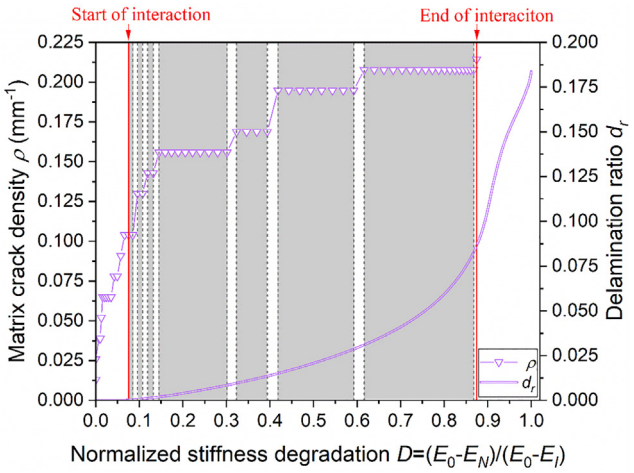

Fig. 12. The growing trends of matrix crack density and delamination ratio with the increase of normalized stiffness degradation within Stage I for specimen #1–2.

Table 3
The fatigue life at the start and end of interaction for all specimens.

Specimen	Group 1				Group 2		
	#1–1	#1–2	#1–3	#1–4	#2–1	#2–2	#2–3
Start	3500	9000	4500	5500	10,500	22,500	18,000
End	28,000	32,000	20,500	26,500	53,500	42,000	50,000

area fluctuated within 15% according to the range of Poisson's ratio, *i.e.* 0.023–0.1 (see Fig. 7(a) and Fig. 8(a)). The co-existing of both transverse matrix cracks and delamination indicates the existence of interactive periods between both damage mechanisms, which might cause the differences of damage accumulation process for specimens with similar stiffness degradation and thus need to be further explored.

Fig. 9 plots the growing trend of delamination ratio d_r with matrix crack density ρ. For both groups, most of specimens experienced an exponential increase of d_r when ρ was larger than a certain threshold, approximately 0.1 mm^{-1} for specimen #1-1/#1-2/#2-1, 0.15 mm^{-1} for specimen #1-4/#2-3 and 0.25 mm^{-1} for specimen #1-3/#2-2. The lower this threshold was, the higher the d_r was for the same matrix crack density within each group. This fact triggered different levels of

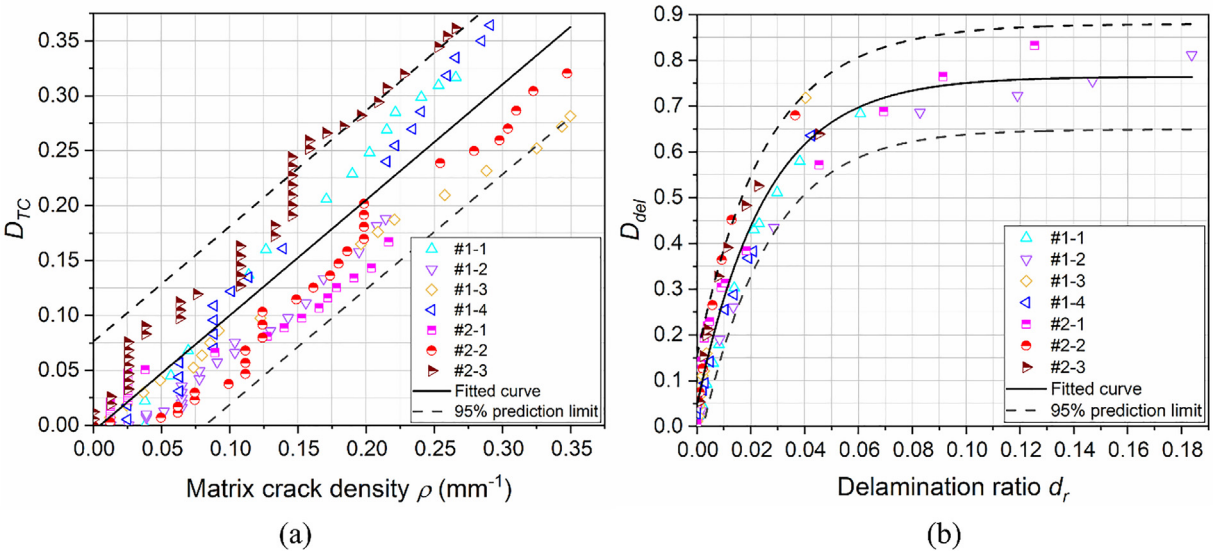

Fig. 13. The plots of normalized stiffness degradation contributed by transverse matrix cracks with matrix crack density (a); the plots of normalized stiffness degradation contributed by delamination with delamination ratio (b).

interactions between transverse matrix cracks and delamination, leading to different accumulation of both damage mechanisms for each group. As a result, specimens with larger d_{rs} (*i.e.* delamination ratio at CDS) showed lower ρ_s. The results reflect the constraining effect of delamination on the generation of new transverse matrix crack as reported in literature [2,17,21], which then postpones the occurrence of CDS.

In the same range of ρ_s, wider scatter band of d_{rs} was presented for the specimens at Group 1 (see Fig. 9), which indicates the severer interactive levels between both damage mechanisms for specimens with lower initial fatigue resistance. Besides, the lowest level of interaction can be regarded as specimen #1-3 due to the negligible d_{rs}. To quantify the severity of interactive levels between both damage mechanisms, the proposed crack growth factor a was related to matrix crack density and delamination ratio at CDS. In Fig. 10, a linear increase of ρ_s as a function of a is presented for both groups, while d_{rs} shows a non-linear decreasing trend with the increase of a. For both groups, lower a corresponds to more significant interaction between transverse matrix cracks and delamination as a result of lower matrix crack density and higher delamination ratio, and vice versa.

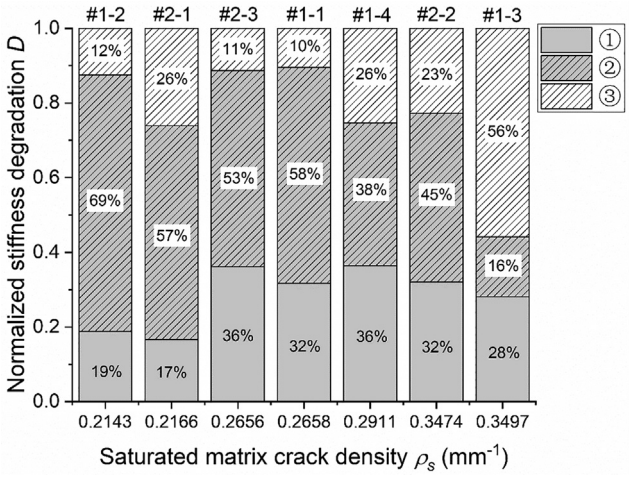

Fig. 14. The proportions of normalized stiffness degradation separately induced by transverse matrix cracks and delamination within Stage I for all specimens. (①: D_{TC} at CDS; ②: D_{del} at CDS; ③: the increment of D_{del} from CDS to the end of Stage I).

In order to explore further the interaction between both damage mechanisms, the growth rates of matrix crack density $\Delta\rho/\Delta N$and delamination ratio $\Delta d_r/\Delta N$ with increase of N are presented in Fig. 11. $\Delta\rho/\Delta N$ was obtained from the fitting function $\rho(N)$ (see Fig. 4). Considering the remarkably slow accumulation process of transverse matrix cracks during the first 6500 cycles for specimens of Group 2 (see Fig. 4(b)), the corresponding $\Delta\rho/\Delta N$ was zero here. A decreasing trend is showed for $\Delta\rho/\Delta N$, and the larger the a (see Table 2) is, the accumulation of transverse matrix cracks happens faster. This fact highlights that a represents the growing trend of matrix crack density. Different from $\Delta\rho/\Delta N$, $\Delta d_r/\Delta N$ experienced an increasing trend followed by a gradual decrease till the end of Stage I for most of specimens. The highest $\Delta d_r/\Delta N$ appeared around CDS (marked as stars in Fig. 11(b)) except specimen #1-3 which had a continuously linear increase as a consequence of low-level interaction between both damage mechanisms. A relatively slow growth rate for both matrix crack density and delamination ratio were observed for specimen of Group 2, presenting the consistency of accumulation rate of both damage mechanisms with the degradation rate of stiffness. Within each group, specimens with high $\Delta\rho/\Delta N$ usually accompanied with low $\Delta d_r/\Delta N$, which reflects the constraints between both damage mechanisms.

3.4. Decoupling of stiffness degradation related to individual damage mechanics

Seeking to understand the accumulation and interaction of transverse matrix cracks and delamination, the contribution of each damage mechanism on stiffness degradation during Stage I should be decoupled.

Fig. 12 shows the increase of matrix crack density ρ and delamination ratio d_r as a function of stiffness degradation D for specimen #1-2. D is calculated by $(E_0\text{-}E_N)/(E_0\text{-}E_I)$ where E_I is the dynamic stiffness at the end of Stage I. To decouple D, the first step is to quantify the interaction period at Stage I, where it is assumed that one damage mechanism played the dominant role to degrade stiffness at each moment. Delamination controlled D at the flat section of ρ (see the grey region in Fig. 12), while transverse matrix cracks were the dominant contributor to D at the section where ρ increased rapidly and the effect of delamination on D is ignored in view that d_r had a slight increase (see the white region in Fig. 12). As a result, the start of interaction is defined at the moment when ρ remains constant and d_r is larger than zero, while the end of interaction is exactly at CDS, as marked in Fig. 12. After CDS,

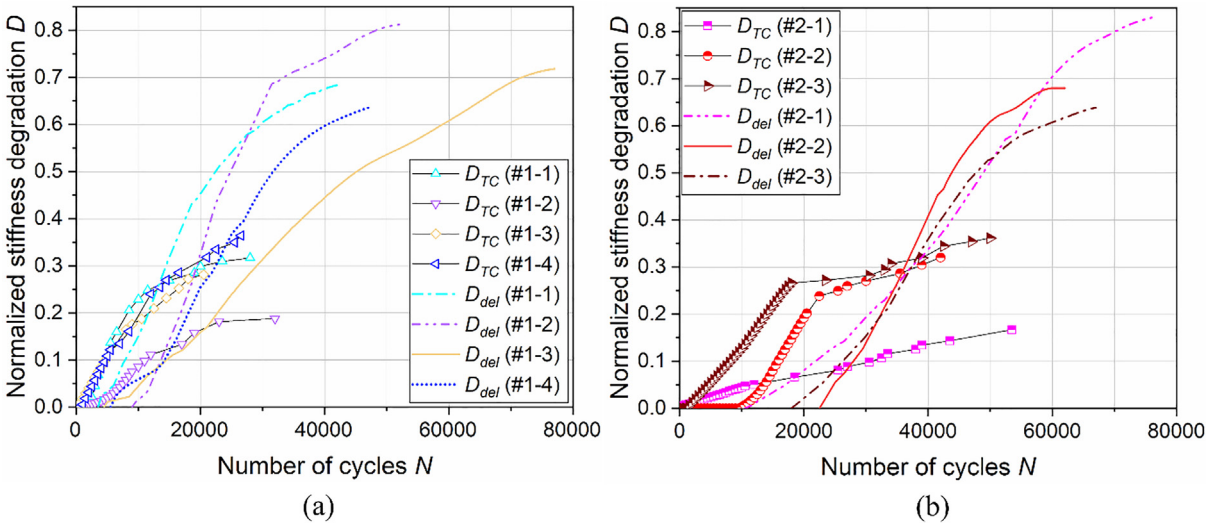

Fig. 15. The growing trends of normalized stiffness degradation separately induced by transverse matrix cracks and delamination with the increase of fatigue life for specimens of Group 1 (a) and Group 2 (b).

delamination, as the only active damage mechanism, continued to affect D. Table 3 lists the fatigue life at the start and end of interaction period for all specimens.

Based on what is proposed above, the growing trend of decoupled stiffness degradation, D_{TC} and D_{del} for transverse matrix cracks and delamination respectively, is shown in Fig. 13. A linear increase of D_{TC} is obtained with the increase of ρ, which is also reported by Wharmby *et al.* [29] As for D_{del}, a non-linear increase with d_r is presented for all specimens and the growing trend of D_{del} converges, indicating the existence of a threshold for which further growing of delamination does not affect the stiffness.

In addition, the contributions of transverse matrix cracks and delamination on the stiffness degradation at CDS and from CDS to Stage I are quantified in Fig. 14. For all specimens, the majority of stiffness within Stage I was degraded because of the delamination (see the shadow region) rather than the transverse matrix cracks (see the non-shadow region). Although this observation contradicts part of the literature, which reports that transverse matrix cracks are the dominant damage mechanism for the stiffness degradation during the fatigue life [16,17,26], the delamination's dominance can be attributed to the ply-block of the 90° plies. Until CDS, larger portion of stiffness degradation was produced by transverse matrix cracks (see Region ①), accompanying with less amount induced by delamination (see Region ②) for specimens with higher saturated matrix crack density ρ_s. This result reflects the competitive relation between the two damage mechanisms to degrade stiffness. From CDS to the end of Stage I, the stiffness degradation, caused by delamination, was lower at Region ③ than that at Region ②. Only specimen #1-3 showed the opposite phenomenon due to the less significant interaction between both damage mechanisms compared with other specimens.

Fig. 15 shows the non-linear growing trends of D_{TC} and D_{del} as a function of N. Compared with Group 1, a slower increase of both D_{TC} and D_{del} with number of cycles was observed for specimens of Group 2 with the slower accumulation process of both damage mechanisms and higher fatigue resistance. As D_{del} increased, the growing rate of D_{TC} decreased due to the restriction from delamination and this fact is evident for the specimens of Group 2 than that of Group 1. After CDS, as a result of the shielding effect between delamination tips propagating towards each other [26], D_{del} was constant within 20,000 cycles for most of specimens with significant interaction between both damage mechanisms.

4. Conclusions

The accumulation and interaction of transverse matrix cracks and delamination in early fatigue life are characterized and quantified for CFRP cross-ply laminates. The contribution of each damage mechanism on stiffness degradation is also analysed. The main conclusions are listed as follows:

(1) Until the end of Stage I, stiffness degrades about 8% to 11% and two groups of decreasing trends are obtained among specimens.
(2) In-situ Poisson's ratio at the exterior 0-ply and delamination obtained from C-scanning are correlated with each other through the DIC-based transverse strain concentrations, but the former cannot fully represent the early propagation of delamination concentrated near the edges. The inter-laminar crack ratio I_r is introduced, measured by the edge cameras, in order to calculate the delamination near the edges.
(3) For specimens where stiffness degrades slower, both damage mechanisms also show relatively slower growth rates and longer fatigue life is consumed to reach CDS.
(4) Among specimens with similar stiffness degradation, different accumulation process and interactive levels of transverse matrix cracks and delamination are presented. Lower saturated matrix crack density coexists with larger delamination ratio at CDS, and it takes longer fatigue life to reach CDS.
(5) The crack growth factor a can be used to quantify the growth rate of matrix crack density and the interactive levels between both damage mechanisms. Low a corresponds to slow accumulation of transverse matrix cracks and significant interaction between both damage mechanisms.
(6) Delamination is responsible for larger stiffness degradation than transverse matrix cracks at Stage I. This observation is attributed to the ply-block of 90° plies. A linear increase of stiffness degradation is obtained with the increase of matrix crack density, while the growing trend of stiffness degradation due to delamination converges with the increase of delamination ratio.

Declaration of Competing Interest

The authors declare that they have no known competing financial interests or personal relationships that could have appeared to influence the work reported in this paper.

Acknowledgments

The authors would like to thank the financial supports of the China Scholarship Council (No. 201706290028).

References

[1] Reifsnider KL, Jamison R. Fracture of fatigue-loaded composite laminates. Int J Fatigue 1982;4:187–97. https://doi.org/10.1016/0142-1123(82)90001-9.
[2] Pakdel H, Mohammadi B. Characteristic damage state of symmetric laminates subject to uniaxial monotonic-fatigue loading. Eng Fract Mech 2018;199:86–100. https://doi.org/10.1016/j.engfracmech.2018.05.007.
[3] Pakdel H, Mohammadi B. Stiffness degradation of composite laminates due to matrix cracking and induced delamination during tension-tension fatigue. Eng Fract Mech 2019;216:106489https://doi.org/10.1016/j.engfracmech.2019.106489.
[4] Huang J, Pastor ML, Garnier C, Gong XJ. A new model for fatigue life prediction based on infrared thermography and degradation process for CFRP composite laminates. Int J Fatigue 2019;120:87–95. https://doi.org/10.1016/j.ijfatigue.2018.11.002.
[5] Li Y, Zhang R, Li L, Bao P, Zhang W, Yang Z, et al. Temperature variation and damage characteristic of impacted CFRP laminate using infrared thermography : Experimental investigation. Int J Fatigue 2018;112:130–7. https://doi.org/10.1016/j.ijfatigue.2018.03.009.
[6] Naderi M, Kahirdeh A, Khonsari MM. Composites : Part B Dissipated thermal energy and damage evolution of Glass / Epoxy using infrared thermography and acoustic emission. Compos Part B 2012;43:1613–20. https://doi.org/10.1016/j.compositesb.2011.08.002.
[7] Wang S, Shui X, Fu X, Chuang DDL. Early fatigue damage in carbon-fibre composites observed by electrical resistance measurement. J Mater Sci 1998;33:3875–84. https://doi.org/10.1023/A:100467202.
[8] Nevadunsky JJ, Lucas JJ. Early Fatigue Damage Detection in Composite Materials AT1GUEBEHAVIOROF. J Compos Mater 1975;9:394–408. https://doi.org/10.1177/002199837500900409.
[9] Berthelot J-M, Ei Mahi A, Le Corre J-F. Development of transverse cracking in cross-ply laminates during fatigue tests. Compos Sci Technol 2001;61:1711–21. https://doi.org/10.1016/S0266-3538(01)00068-9.
[10] Maragoni L, Carraro PA, Peron M, Quaresimin M. Fatigue behaviour of glass / epoxy laminates in the presence of voids. Int J Fatigue 2017;95:18–28. https://doi.org/10.1016/j.ijfatigue.2016.10.004.
[11] Quaresimin M, Carraro PA, Maragoni L. Early stage damage in off-axis plies under fatigue loading. Compos Sci Technol 2016;128:147–54. https://doi.org/10.1016/j.compscitech.2016.03.015.
[12] Alderliesten RC, Brunner AJ, Pascoe JA. Cyclic fatigue fracture of composites : What has testing revealed about the physics of the processes so far ? Eng Fract Mech 2018;203:186–96. https://doi.org/10.1016/j.engfracmech.2018.06.023.
[13] Qi W, Yao W, Shen H. A bi-directional damage model for matrix cracking evolution in composite laminates under fatigue loadings. Int J Fatigue 2020;134.. https://doi.org/10.1016/j.ijfatigue.2019.105417.
[14] Jagannathan N, Gururaja S, Manjunatha CM. Probabilistic strength based matrix crack evolution model in multi- directional composite laminates under fatigue loading. Int J Fatigue 2018;117:135–47. https://doi.org/10.1016/j.ijfatigue.2018.08.016.
[15] Glud JA, Dulieu-barton JM, Thomsen OT, Overgaard LCT. Composites : Part A Fatigue damage evolution in GFRP laminates with constrained off-axis plies. Compos Part A 2017;95:359–69. https://doi.org/10.1016/j.compositesa.2017.02.005.
[16] Li C, Ellyin F, Wharmby A. On matrix crack saturation in composite laminates. Compos Part B Eng 2003;34:473–80. https://doi.org/10.1016/S1359-8368(03)00020-9.
[17] Shen H, Yao W, Qi W, Zong J. Experimental investigation on damage evolution in cross-ply laminates subjected to quasi-static and fatigue loading. Compos Part B 2017;120:10–26. https://doi.org/10.1016/j.compositesb.2017.02.033.
[18] Hosoi A, Sakuma S, Fujita Y, Kawada H. Composites : Part A Prediction of initiation of transverse cracks in cross-ply CFRP laminates under fatigue loading by fatigue properties of unidirectional CFRP in 90 ° direction. Compos Part A 2015;68:398–405. https://doi.org/10.1016/j.compositesa.2014.10.022.
[19] Hosoi A, Takamura K, Sato N, Kawada H. Quantitative evaluation of fatigue damage growth in CFRP laminates that changes due to applied stress level. Int J Fatigue 2011;33:781–7. https://doi.org/10.1016/j.ijfatigue.2010.12.017.
[20] Xu L. Interaction between matrix cracking and edge delamination in composite laminates. Compos Sci Technol 1994;50:469–78. https://doi.org/10.1016/0266-3538(94)90055-8.
[21] Talreja R. Damage and fatigue in composites – A personal account. Compos Sci Technol 2008;68:2585–91. https://doi.org/10.1016/j.compscitech.2008.04.042.
[22] Samareh-mousavi SS, Taheri-behrooz F. A novel creep-fatigue stiffness degradation model for composite materials. Compos Struct 2020;237:111955https://doi.org/10.1016/j.compstruct.2020.111955.
[23] Taheri-behrooz F, Shokrieh MM, Lessard LB. Residual stiffness in cross-ply laminates subjected to cyclic loading. Compos Struct 2008;85:205–12. https://doi.org/10.1016/j.compstruct.2007.10.025.
[24] Samareh-mousavi SS, Mandegarian S, Taheri-behrooz F. A nonlinear FE analysis to model progressive fatigue damage of cross-ply laminates under pin-loaded conditions. Int J Fatigue 2019;119:290–301. https://doi.org/10.1016/j.ijfatigue.2018.10.010.
[25] Shabani P, Taheri-behrooz F, Maleki S, Hasheminasab M. Life prediction of a notched composite ring using progressive fatigue damage models. Compos Part B 2019;165:754–63. https://doi.org/10.1016/j.compositesb.2019.02.031.
[26] Carraro PA, Maragoni L, Quaresimin M. Characterisation and analysis of transverse crack-induced delamination in cross-ply composite laminates under fatigue loadings. Int J Fatigue 2019;129:105217https://doi.org/10.1016/j.ijfatigue.2019.105217.
[27] Shokrieh MM, Taheri-Behrooz F. Progressive Fatigue Damage Modeling of Cross-ply Laminates, I: Modeling Strategy. J Compos Mater 2010;44:1217–31. https://doi.org/10.1177/0021998309351604.
[28] Shokrieh MM, Taheri-Behrooz F, Lessard LB. Progressive Fatigue Damage Modeling of Cross-ply Laminates, II: Experimental Evaluation. J Compos Mater 2010;44:1261–77. https://doi.org/10.1177/0021998309351605.
[29] Wharmby AW, Ellyin F, Wolodko JD. Observations on damage development in fibre reinforced polymer laminates under cyclic loading. Int J Fatigue 2003;25:437–46. https://doi.org/10.1016/S0142-1123(02)00118-4.
[30] Wharmby AW, Ellyin F. Damage growth in constrained angle-ply laminates under cyclic loading. Compos Sci Technol 2002;62:1239–47. https://doi.org/10.1016/S0266-3538(02)00075-1.
[31] Ma D, Manes A, Amico SC, Giglio M. Ballistic strain-rate-dependent material modelling of glass-fibre woven composite based on the prediction of a meso-heterogeneous approach. Compos Struct 2019;216:187–200. https://doi.org/10.1016/j.compstruct.2019.02.102.
[32] Takeda N, Ogihara S, Kobayashi A. Microscopic fatigue damage progress in CFRP cross-ply laminates. Composites 1995;26:859–67. https://doi.org/10.1016/0010-4361(95)90879-5.
[33] Kobayashi S, Takeda N. Experimental and analytical characterization of transverse cracking behavior in carbon / bismaleimide cross-ply laminates under mechanical fatigue loading. Compos Part B Eng 2002;33:471–8. https://doi.org/10.1016/S1359-8368(02)00028-8.
[34] Llobet J, Maimí P, Essa Y, De FM. Progressive matrix cracking in carbon / epoxy cross-ply laminates under static and fatigue loading. Int J Fatigue 2019;119:330–7. https://doi.org/10.1016/j.ijfatigue.2018.10.008.
[35] Vahid Movahedi-rad A, Keller T, Vassilopoulos AP. Interrupted tension-tension fatigue behavior of angle-ply GFRP composite laminates. Int J Fatigue 2018;113:377–88. https://doi.org/10.1016/j.ijfatigue.2018.05.001.
[36] Vahid Movahedi-rad A, Keller T, Vassilopoulos AP. Creep effects on tension-tension fatigue behavior of angle-ply GFRP composite laminates. Int J Fatigue 2019;123:144–56. https://doi.org/10.1016/j.ijfatigue.2019.02.010.
[37] Hexcel. HexPly ® 6376 - Product Data Sheet - EU Version 2016:1–2.
[38] Kupski J, Teixeira De Freitas S, Zarouchas D, Camanho PP, Benedictus R. Composite layup effect on the failure mechanism of single lap bonded joints. Compos Struct 2019;217:14–26. https://doi.org/10.1016/j.compstruct.2019.02.093.
[39] ASTM International. D3479/D3479M-19 Standard Test Method for Tension-Tension Fatigue of Polymer Matrix Composite Materials. West Conshohocken, PA; ASTM Int 2019. doi:10.1520/D3479_D3479M-19.
[40] Vahid Movahedi-Rad A, Keller T, Vassilopoulos AP. Fatigue damage in angle-ply GFRP laminates under tension-tension fatigue. Int J Fatigue 2018;109:60–9. https://doi.org/10.1016/j.ijfatigue.2017.12.015.
[41] Maier J, Pinter G. 15 - Stiffness-based approach to fatigue-life prediction of composite materials, vol. c., 2nd ed. Elsevier Ltd.; 2020. https://doi.org/10.1016/B978-0-08-102575-8.00015-2.
[42] Wang CH. Introduction To Fracture Mechanics. 1996. https://doi.org/10.13140/RG.2.1.1444.2408.
[43] Oz FE, Ersoy N, Mehdikhani M, Lomov SV. Multi-instrument in-situ damage monitoring in quasi-isotropic CFRP laminates under tension. Compos Struct 2018;196:163–80. https://doi.org/10.1016/j.compstruct.2018.05.006.
[44] O'Brien TK. Characterization of Delamination Onset and Growth in a Composite Laminate. In: Reifsnider K, editor. Damage Compos. Mater. Basic Mech. Accumulation, Toler. Charact. West Conshohocken, PA: ASTM International; 1982. p. 140–67. https://doi.org/10.1520/STP34325S.